Adsorption (2014) 20:427–437
DOI 10.1007/s10450-013-9589-1

Branched versus linear alkane adsorption in carbonaceous slit pores

A. Harrison · R. F. Cracknell · J. Krueger-Venus · L. Sarkisov

Received: 18 May 2013 / Accepted: 7 October 2013 / Published online: 20 October 2013

Abstract The presence of carbonaceous deposits on the internal surfaces of a spark ignition engine has been linked in the literature to impaired vehicle performance, as manifested by increased knocking, higher fuel consumption, higher emissions and other adverse effects. One of the proposed mechanisms, in which the deposits affect the processes in the engine, is the adsorption and desorption of fuel components in the pores within the deposit. In this article we investigate this mechanism in more detail by considering single component adsorption of normal and branched alkanes in selected model slit pores representing the structure of the deposits. We further extend these studies to the binary mixture of normal heptane and isooctane, corresponding to a primary reference fuel blend. In particular, we show that in larger pores adsorption selectivity towards isooctane is about 1.2 on average throughout the pressure range. However, in the smaller 10 Å pore selectivity towards isooctane can be in excess of three as a result of packing effects. These results are then placed in the context of engine performance issues.

Electronic supplementary material The online version of this article (doi:10.1007/s10450-013-9589-1) contains supplementary material, which is available to authorized users.

A. Harrison · L. Sarkisov (✉)
Institute for Materials and Processes, The University of Edinburgh, Edinburgh, UK
e-mail: lev.sarkisov@ed.ac.uk

R. F. Cracknell
Shell Projects and Technology, Shell Technology Centre Thornton, Chester, UK

J. Krueger-Venus
Shell Projects and Technology, Shell Global Solutions (Deutschland) GmbH, Hamburg, Germany

Keywords Adsorption · Simulation · Slit pore · Alkane · Branched · Engine deposit

1 Introduction

This article continues a series of recent publications aimed at understanding adsorption phenomena in engine deposits (Pinto da Costa et al. 2009, 2011). These deposits are mainly carbonaceous materials which accumulate on the majority of the surfaces inside the internal gasoline combustion engine. The mechanism of their formation is not yet clearly understood. However, it is generally accepted that they derive primarily from the incomplete combustion of some of the fuel components and fuel additives (Kalghatgi 1990, 1995). Engine deposits are highly heterogeneous porous materials, both structurally and chemically, with carbon constituting only between 65 and 75 % of the material by weight depending on its location in the engine and other parameters (Pinto da Costa et al. 2011; Shu et al. 2012).

Accumulation of these deposits has been linked with deterioration in engine performance, including slower response of the car when the accelerator is depressed, higher fuel consumption, and higher gaseous emissions (Kalghatgi 1990, 1995, 1996). In the most adverse scenario, presence of the deposits increases propensity of the engine to knock. Several mechanisms have been identified, in which the deposits affect the processes in the engine. The nature of these mechanisms and their relative importance strongly depend on the location of the deposits. Deposits located in the combustion chamber [combustion chamber deposits (CCDs)] and on the surfaces of the intake valves [intake valve deposits (IVDs)] have been recognized as the main contributors to the performance deterioration

(Kalghatgi 1995). One of the identified mechanisms responsible for this deterioration is the adsorption of fuel components due to the highly porous nature of the deposits (Heywood 1988; Kalghatgi 1995; Zerda et al. 1999). As a result, this may lead to substantial variations in the composition of the fuel–air mixture, adversely affecting the course and patterns of the combustion reactions. At the same time, fuel components adsorbed prior to ignition and then desorbed at later cycles of the process contribute to higher emissions of gaseous hydrocarbons and higher fuel consumption (Shibata et al. 1992; Houser and Crosby 1992).

In our previous studies we set to investigate the role of this mechanism in more detail (Pinto da Costa et al. 2009, 2011). The processes inside the engine compartments are immensely complex, involving hundreds of species and chemical reactions with substantial spatial and temporal variations in temperature and pressure. Accurate replication of these processes in a laboratory study is impracticable and a simplified system is required. As a starting point it is important to consider interaction of individual species, representing the fuel mixture, with the deposits at a particular static value of temperature and pressure. Even this simplified task presents a substantial challenge as the measurement of adsorption of complex species at elevated temperatures and pressures is a difficult experiment. Hence our strategy is to perform a small set of experimental measurements for species and conditions where these measurements are less difficult, use this data to construct and calibrate a predictive molecular model and then employ this model to explore adsorption of selected fuel components under conditions of interest.

To construct this predictive model we adopted a strategy developed over the years in the studies of activated carbons, based on a combination of a limited number of experimental measurements and molecular simulation (Davies and Seaton 1999; Davies et al. 1999; Do and Do 2003). Briefly, within this approach the structure of an activated carbon material is considered as an ensemble of independent slit pores of different widths, which is a reasonable assumption for a number of activated carbons featuring lamellar pore structure. According to this model the adsorption in a real sample is a reflection of a combined adsorption in different pores of this ensemble, with various pore sizes being represented in the material according to the pore size distribution (PSD). Application of this strategy to construct a predictive model of adsorption for an activated carbon would then typically involve the following steps. A single component adsorption isotherm is measured for a sample of activated carbon using some representative species. At the same time, molecular simulations are used to generate a kernel, or in other words a collection, of adsorption isotherms for this species at the same conditions for model slit pores of all widths within the ensemble. A regularization procedure is used to find the most accurate PSD which is compatible with the experimental data. In order to predict adsorption at different conditions, adsorption of new species or a mixture of species, molecular simulations are used again to generate adsorption isotherms in individual slit pores. This data is then combined with the PSD to obtain a prediction of adsorption in a real sample. Seaton et al. (1989) and Ravikovitch et al. (2000) have made substantial contributions in the field by developing reliable procedures for obtaining PSDs. For a simple overview of the issues related to the extraction of a reliable PSD, different methods and regularization protocols the reader is referred to the review by (Vega 2007).

An extension of this strategy to engine deposits must start with the recognition of the important differences between activated carbons and the deposits. Although transmission electron microscopy (TEM) images suggest that some deposits also feature lamellar structure (Zerda et al. 1999) and therefore a slit pore model is a reasonable starting point, the density of the deposits and the chemical composition deviates substantially from the typical characteristics of activated carbons. In our previous studies we used ethane adsorption at ambient temperature to construct and calibrate the predictive model, since ethane is a simple molecule, it is a gas at ambient conditions and at the same time, being a hydrocarbon, it represents the chemistry of fuel components (Pinto da Costa et al. 2009, 2011). We showed that to obtain a reliable PSD it is important to optimize the parameters of the solid–fluid interaction and consider a wider range of pore widths in the kernel. The model was validated using adsorption of ethane at a different temperature and by comparing predicted and experimentally measured adsorption isotherms for normal butane and isobutane at ambient temperatures. We considered three samples of the deposits (two CCDs and one IVD) and although they featured different PSDs, the parameters of the molecular simulation models were shown to be transferable between the samples.

All the PSDs thereby obtained featured a peak around 10 Å and one or several peaks between 30 and 50 Å, depending on the sample. The PSDs were used to predict equilibrium adsorption of fuel components in the deposits under relevant conditions. In studies of engine performance various mixtures of 2,2,4-trimethylpentane (isooctane, octane number 100) and *n*-heptane (octane number 0) are quite often used as model or reference fuels. Hence, in our preliminary studies we focused on single component isotherms of these species. The choice of the temperature for adsorption predictions was dictated by the typical temperatures observed on the surfaces of the engine. The lowest surface temperature around 390 K is observed in the end

gas region, while the highest temperature is observed on the surface of the exhaust valve and can reach 1,000 K (Heywood 1988). In comparison, temperatures on the intake valve are much lower (also around 390 K) (Kalghatgi 1995). The temperature of the piston top surface varies between 420 and 500 K. Adsorption predictions were carried out at temperatures corresponding to the lowest typical surface temperatures observed during the engine cycle (390 and 420 K), as this would allow us to establish the extent of adsorption under the most favourable conditions (Pinto da Costa et al. 2011).

Our studies demonstrated that a substantial amount of alkane species can be adsorbed by the deposits (Pinto da Costa et al. 2011). According to these predictions, in the equilibrium limit the IVDs present in the engine may have the capacity to adsorb more fluid than the amount of fuel introduced to the engine during one cycle (see an example calculation in the Supplementary Information file). Hence, if this effect develops even to a fraction of the equilibrium extent, it may have important repercussions for the operation of the engine. We further observed that the deposits exhibit higher affinity towards the adsorption of isooctane compared to normal heptane.

This latter effect may also have important consequences for the composition of the mixture during transient operation biasing it towards alkane species with lower octane ratings. In this article, we investigate this effect in further detail, by considering single component and binary mixture adsorption of several linear and branched alkanes in model slit pores. Aside from the practical application of interest here, this study may also provide some fundamental insights on the behaviour of confined alkanes. Although adsorption of linear and branched alkanes has been extensively investigated in the context of catalytic cracking and separations in zeolites, slit pore geometries have received substantially less attention. Severson and Snurr have recently performed an extensive simulation study of alkanes adsorption in carbon slit pores Severson and Snurr (2007). Adsorption of linear alkanes (from ethane to pentadecane) has been explored as a function of chain length, pore width and temperature (Severson and Snurr 2007). Vapour–liquid phase behaviour, critical properties and surface tension of linear alkanes (from methane to normal octane) under confinement in slit pores have been recently investigated by Singh et al. (2009). In particularly, similarly to the confined phase behaviour of simple fluids, the authors observed depression of the vapour–liquid critical temperatures to lower values, compared to the bulk system, with the extent of depression enhanced by stronger confinement (Singh et al. 2009). Studies of binary and multicomponent mixtures of alkanes in slit pores are rare and their behaviour has not been explored in any appreciable detail. However, the existing studies suggest that these systems may exhibit a number of interesting effects. Tan and Gubbins considered adsorption of binary mixtures of methane and ethane as a function of carbon slit pore width, temperature and mixture composition using non-local density functional theory (Tan and Gubbins 1992). In the zero pressure regime, selectivity of ethane exhibited a pronounced maximum as a function of pore width, whereas for finite pressures and loadings several distinct types of selectivity isotherms have been identified, depending on the temperature and the location of the conditions with respect to the bulk phase diagram (Tan and Gubbins 1992). Cracknell et al also investigated selectivity for methane-ethane mixtures in slit pores, using grand canonical Monte Carlo simulations, and observed a number of interesting phenomena, associated with the geometric arrangements of diatomic molecules in narrow pores (Cracknell et al. 1994). This work was further extended to ethane–propane binary mixtures. It was demonstrated that molecular species may exhibit an additional range of packing effects, leading to new types of selectivity isotherms, not observed by Tan and Gubbins (Cracknell and Nicholson 1994).

Here we investigate adsorption of *n*-butane, isobutane (i-butane), *n*-heptane, *n*-octane and isooctane (i-octane) at 390 K, which corresponds to the lowest temperature value relevant for the engine operation and considered so far. Butanes are selected as the simplest alkane species, for which the effect of branching can be studied. Normal heptane and i-octane are considered as representative fuel components, and *n*-octane is used to highlight the effect of branching on adsorption properties of i-octane. We focus only on three pores of a specific width. Pores of 10 Å in width are typically present in all types of deposits, 40 Å pore is selected to represent a characteristic width from the 30–50 Å range, while 20 Å pores do not exist in the deposits, but this width is selected to understand any possible transitions in the adsorption regimes between 10 and 40 Å pores. We extend these studies to a binary mixture of *n*-heptane and i-octane, using a typical reference fuel composition, and investigate adsorption of the mixture at 390 K as a function of pore width. Finally, we briefly explore adsorption hysteresis effect, observed for the cases where capillary condensation of adsorbing species takes place.

2 Methodology

The setup for our simulations resembles the one recently employed by Severson and Snurr (Severson and Snurr 2007). A model slit pore in this study consists of two walls, where each wall is made of six graphene layers. Within the walls the layers are separated from each other by 3.35 Å. Slit pores of three different widths, namely 10, 20 and

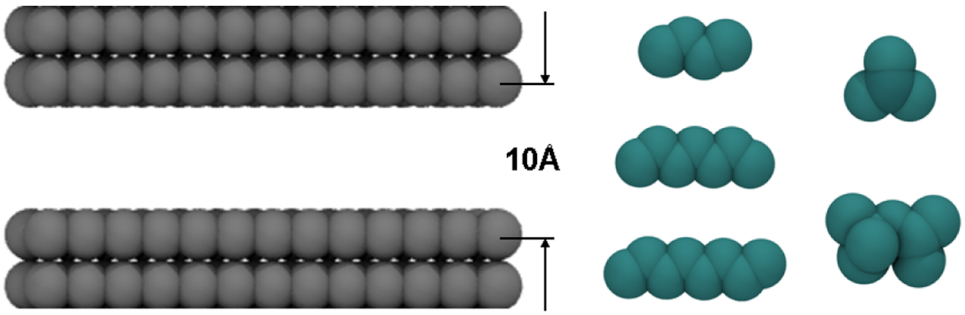

Fig. 1 Schematic visualization of the 10 Å slit pore model (on the *left side*). Only two layers of each wall shown, whereas in the actual model each wall consists of six layers. United atom representations of the adsorbate species considered in these work (on the *right side*). First *column* corresponds to normal butane, heptane and octane from *top down*, whereas two species on the *right* are isobutane (*top*) and isooctane (*bottom*), respectively

40 Å, are considered, with this distance corresponding to the distance in z direction between the centres of the atoms of the inner graphene layers, as shown in Fig. 1. In x and y directions, each pore has dimensions of 31.73 and 34.08 Å, respectively.

Single component adsorption of normal butane (*n*-butane), isobutane (i-butane), normal heptane (*n*-heptane), normal octane (*n*-octane), isooctane (i-octane) and selected binary mixtures of these components are considered. These species are modelled using the TraPPE united atom forcefield (Martin and Siepmann 1998, 1999). For the atoms constituting the walls of the slit pores we adopt parameters from the previous work of Pinto da Costa et al. (2009, 2011). Standard Lorenz-Berthelot rules are applied to generate Lennard-Jones parameters for the interactions between the adsorbing species and the atoms of the slit pore walls. For adsorbate-adsorbate interactions potential cut-off distance of 15 Å is imposed. The system is placed in periodic boundary conditions in x and y directions.

All grand canonical Monte Carlo simulations are performed using the Multipurpose Simulation Code, MuSiC (Gupta et al. 2003). For linear alkanes we employ configurational bias Monte Carlo (CB GCMC) combined with the energy bias method (CB/EB GCMC), using the pre-calculated potential maps (Snurr et al. 1993). These maps are generated using 30 Å cut-off for interactions between atoms of the walls and atoms of the adsorbing species. To accommodate this cut-off in the generation of the maps, several replicas of the system are considered in periodic boundary conditions. Each CB/EB GCMC move consists either of insertion, deletion, translation or re-growth attempt, selected with equal weight. Several alternative CB GCMC schemes have been proposed for branched alkanes (Martin and Siepmann 1999; Macedonia and Maginn 1999). For example, in the method by Macedonia and Maginn (1999), an additional simulation is required to generate a library of conformations of the branched fragment of the molecule which is later used in the CB GCMC scheme to assemble the whole molecule together. In case of i-butane, this simply reduces to an insertion of a whole molecule from the library of conformers. Furthermore, i-octane can be considered as an assembly of two branched fragments, requiring two additional simulations for each fragment. It seems highly branched species considered here benefit little from the complicated machinery of CB GCMC approach. Instead, we use a simplified approach, where branched alkane molecules are inserted as rigid structures, selected from a library of conformations, corresponding to the canonical distribution at a particular temperature. For this, we first perform a Molecular Dynamics simulation of a small set of molecules (100–200) in a bulk simulation cell under constant volume and temperature conditions. The temperature of the system is maintained with the Nose-Hoover thermostat (basic principles of various thermostats are considered in Frenkel and Smit 2002). The molecules are treated as ideal gas and only intramolecular interactions are considered. In the second stage, an energy bias grand canonical Monte Carlo (EB GCMC) is performed with the configurations of the molecules tried for insertion drawn from the pre-calculated library. Overall, an EB GCMC move for a branched alkane consists of an insertion, deletion, rotation and translation attempt, selected with equal weights. In the Supplemental Information file we show that in the case of highly branched molecules such as i-octane, this approach is as accurate as CB/EB GCMC.

Each point on the adsorption isotherm is generated using at least 5×10^6 (and up to 1×10^8) moves, with 70 % of them allocated for equilibration. On adsorption, we consider a series of increasing pressure values, and the last configuration from a lower pressure point serves as a starting configuration for the next, higher pressure point. To simulate the desorption process, the protocol is reversed and a simulation consists of a series of decreasing pressure values, again with the configuration of the preceding point used as an input configuration for the following point. This

setup has been employed in several previous studies to investigate hysteresis in slit pores and more complex porous materials (Sarkisov and Monson 2000, 2001).

An adsorption simulation takes fugacity of adsorbing species as an input parameter and returns the absolute amount adsorbed (in terms of number of molecules per simulation cell) as a result. In the results section the isotherms are reported as the excess amount adsorbed versus pressure of adsorbing species. We use the Peng–Robinson equation of state to relate the fugacity and pressure of adsorbing species, and the following expression to obtain the excess amount (Talu and Myers 2001):

$$n^{ex} = n^{abs} - \rho_{bulk} V_p \quad (1)$$

where n^{ex} and n^{abs} are excess and absolute amounts adsorbed, respectively (number of molecules per simulation cell), ρ_{bulk} is the density of the bulk phase at the conditions of interest, calculated using the Peng–Robinson equation of state, and $V_p = L_x \times L_y \times (L_z - 6.1\ \text{Å})$ is the pore volume, with L_x and L_y being the dimensions of the pore in x and y directions, L_z its width in z direction and 6.1 Å being the smallest width of the pore, where adsorption is still possible. This calculation of the pore volume is consistent with the previous studies of adsorption in slit pores (Davies and Seaton 1999). All the simulation parameters employed in these studies are provided in detail in the Supplemental Information file.

3 Results

3.1 Single component studies

We begin our analysis with the single adsorption isotherms for linear and branched butanes. At 390 K, the bulk condensation pressures are about 2,000 and 2,600 kPa for *n*-butane and i-butane, respectively. The adsorption isotherms shown in Figs. 2 and 3 span the pressure range up to the saturation pressure of the species. In Fig. 2, these adsorption isotherms are shown for 10 Å pore using normal and logarithmic pressure scales. Adsorption isotherms have type I shape and the loading of butanes (shown as number of molecules per simulation cell) is very similar for the two isomers. In larger pores (Fig. 3) the shape of the isotherm changes and becomes more linear in the 40 Å pore. In both 20 and 40 Å pores, there is a slightly higher loading of *n*-butane in the whole pressure range. This is a general reflection of the relative bulk properties of the isomers, with *n*-butane being generally closer to the bulk condensation pressure on the presented pressure scale. In the Supplemental Information file (SI) this data is re-plotted using the relative pressure scale (P/P_0, where P_0 is the bulk condensation pressure at 390 K). On this scale the isotherms for the isomers in 20 and 40 Å pores are quite close to each other with a slightly higher loading for i-butane in the pressure range of up to 0.5 P/P_0 in 20 Å and in the whole range of pressures considered in the 40 Å pore.

Higher alkanes exhibit a more complex landscape of behaviour. In Fig. 4, adsorption isotherms for *n*-heptane, *n*-octane and i-octane in 10 Å slit pore are shown. All three species exhibit type I isotherm at these conditions. At lower pressures, as seen on the right panel of Fig. 4, using the logarithmic pressure scale, loading of i-octane is higher than that for *n*-heptane. The loading of i-octane is also very similar to the loading of *n*-octane. In this regime, higher loading of *n*-octane compared to *n*-heptane is an enthalpic effect associated with the presence of an additional alkane group in the octanes. For normal alkanes this trend is in general agreement with the previous observations of Severson and Snurr (Severson and Snurr 2007). At higher pressures, i-octane has higher loadings than both normal alkanes, and this must be a result of a more efficient packing of i-octane in a pore of this particular size. As illustrated in the Supplementary Information file 10 Å can not accommodate formation of two layers of linear alkanes.

Figure 5 shows adsorption isotherms for *n*-heptane, *n*-octane and i-octane in 20 and 40 Å pores at 390 K. From this figure, it is clear that alkanes in carbonaceous slit pores follow general trends for confined fluid phase behaviour. Briefly, confinement in a porous structure shifts condensation of a fluid towards lower pressures. Stronger confinement (smaller pores) shifts this transition further towards lower pressures until capillary transition disappears altogether, which would correspond to the capillary filling regime. A complete phase diagram collected for a slit pore of a particular width will have a shape similar to the bulk phase diagram, but with lower values of critical temperature. A series of isotherms corresponding to different temperatures within the two phase region of the confined phase diagram will feature hysteresis loops associated with the metastability of the confined fluid. These hysteresis loops become smaller in size as the temperature increases and the system approaches the confined fluid critical point.

Indeed, these trends are observed for alkanes here. In both 20 and 40 Å pores all three species undergo capillary condensation, with *n*-octane condensing first followed by i-octane and then *n*-heptane. In the 20 Å pore the location of the capillary condensation is shifted further towards lower values of pressure, compared to 40 Å and in both pores capillary condensation occurs at lower values of pressure, compared to the bulk condensation (169, 79, 163 kPa for bulk *n*-heptane, *n*-octane and i-octane, respectively). In a larger pore, all three species also exhibit substantial desorption hysteresis, whereas in the 20 Å the

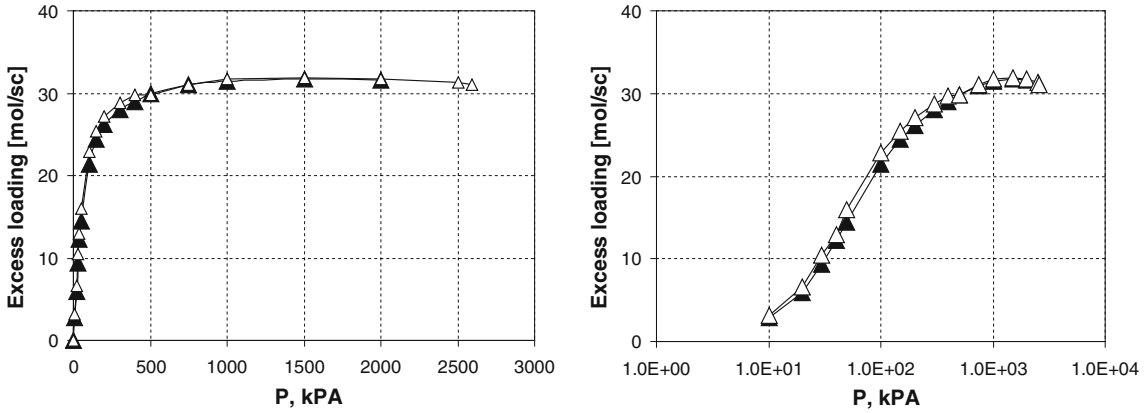

Fig. 2 Adsorption isotherms (number of molecules per simulation cell as a function of pressure) for *n*-butane (*black triangles* and *lines*) and i-butane (*white triangles* and *black lines*) in 10 Å slit pore at 390 K. *Right panel* uses the logarithmic scale for pressure

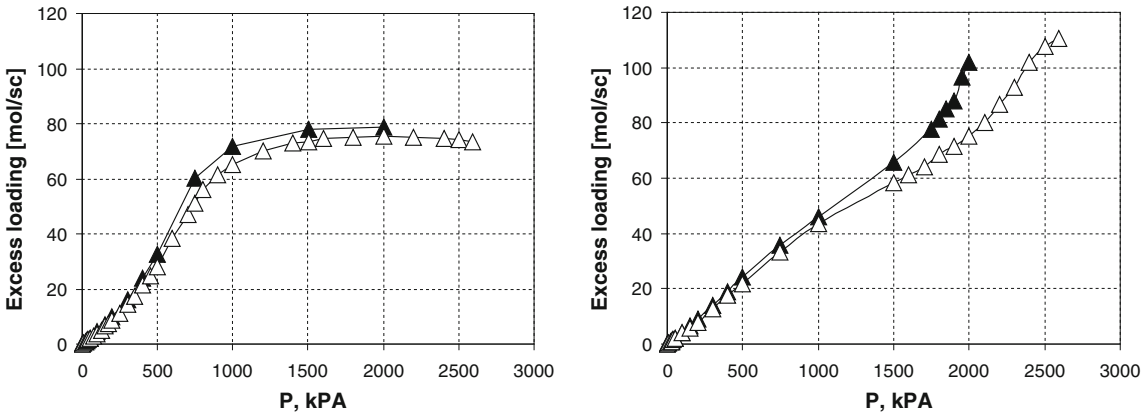

Fig. 3 Adsorption isotherms (number of molecules per simulation cell as a function of pressure) for *n*-butane (*black triangles* and *lines*) and i-butane (*white triangles* and *lines*) in 20 Å slit pore (*left panel*) and 40 Å slit pore (*right panel*) at 390 K

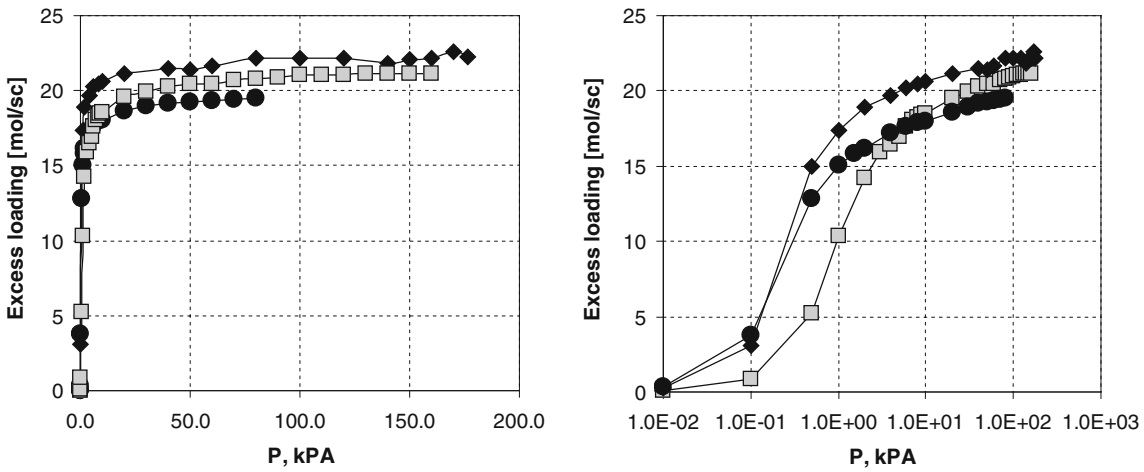

Fig. 4 Adsorption isotherms (number of molecules per simulation cell as a function of pressure) for *n*-heptane (*grey squares* and *lines*) and *n*-octane (*black circle* and *lines*) and i-octane (*black diamonds* and *lines*) in 10 Å slit pore at 390 K. *Right panel* shows the data using the logarithmic pressure scale

transition has no visible hysteresis. It is important to emphasize here that both adsorption and desorption transitions observed here for 40 Å pore are hysteresis transitions and neither of the branches corresponds to the true location of the confined vapour–liquid equilibrium. Following the description of the confined fluid phase

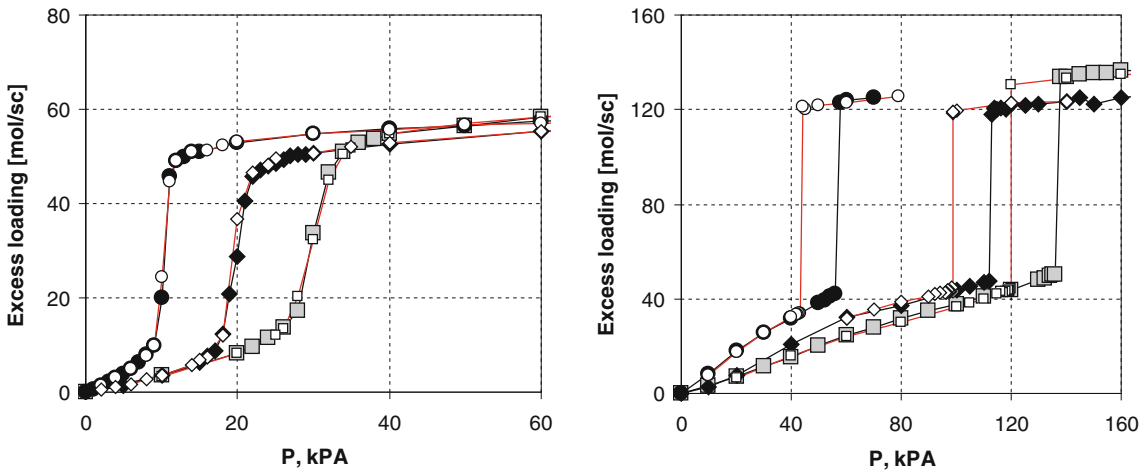

Fig. 5 Adsorption and desorption isotherms (number of molecules per simulation cell as a function of pressure) for *n*-heptane (*grey squares* and *black lines* for adsorption and *white squares* and *red lines* for desorption), *n*-octane (*black circles* and *lines* for adsorption and *white circles* and *red lines* for desorption, respectively) and i-octane (*black diamonds* and *lines* for adsorption and *white diamonds* and *red lines* for desorption, respectively) in 20 Å slit pore (on the *left*) and 40 Å slit pore (on the *right*) at 390 K (Color figure online)

behaviour provided earlier, in 20 Å the temperature of interest (390 K) is much closer to the corresponding critical points of the confined alkanes and the envelopes of metastability are expected to become smaller. We also highlight here that although i-octane initially adsorbs more strongly compared to *n*-heptane (as seen from the earlier capillary condensation), at higher pressures both linear alkanes tend to compact more effectively, compared to i-octane and the density of linear alkanes is slightly higher than that of the branched one. This behaviour in 20 and 40 Å pores is different from that for 10 Å pore.

3.2 Binary mixtures of i-octane and *n*-heptane

Binary mixtures of i-octane and *n*-heptane are often used as primary reference fuels. Here we focus on the adsorption behaviour of just one particular, commonly used composition, with 90 % i-octane 10 % *n*-heptane on a liquid volume basis. The mixture corresponds to 0.89 mol fraction of i-octane. Before we consider the outcomes of the simulations, it is important again to briefly summarize what we might expect to observe. Phase behaviour of confined mixtures has been investigated to a substantially less extent than that for single components (Gelb et al. 1999). In the simplest scenario, one would expect the confined fluid phase diagram to reflect at least some features of the bulk phase behaviour. For example, experimental studies on the liquid-liquid phase coexistence of nitrobenzene and n-hexane mixtures reveal a confined phase diagram similar in shape to the bulk one but with smaller phase envelope. Gibbs ensemble studies of phase behaviour of binary mixtures of CO_2, CH_4, and N_2 suggest that confinement in slit pores leads to the depressed critical point and smaller vapour–liquid envelope compared to the bulk system (Li et al. 2012).

Consider now a bulk mixture of i-octane and *n*-heptane. For simplicity we can treat this mixture as ideal, following Raoult's law. In the bulk phase, on the P−x−y diagram components of an ideal binary mixture form a two phase envelope between the liquid phase and the vapour phase. In the isothermal compression process, which starts from a location in the vapour region of the diagram, the first drop of liquid forms at the pressure dew point. As further compression proceeds, a two phase system is observed for a range of pressures, until condensation completes and only liquid phase is present. In the grand canonical simulation of mixture adsorption, we specify the total pressure of the gas phase and its composition in coexistence with the adsorbent. Using these parameters and an appropriate binary equation of state, fugacities of species in the mixture are obtained, and this is what is used as input in the simulations, formally corresponding to the $\{\mu_1, \mu_2, V, T\}$ ensemble, where μ_1, μ_2 are the chemical potentials of the two co-adsorbing species. As the total pressure of the bulk phase increases, the system undergoes a capillary condensation, similarly to a single component scenario. However, the equilibrium composition of the confined liquid-like phase may be different from the composition of the corresponding vapour-like phase, with this difference directly related to the width of the two phase envelope. Both in bulk and under confinement, the width of the two phase envelope should reflect the differences in thermodynamic properties of the fluids in the mixture, and species with a high relative volatility should form a wide two phase region. For species of similar relative volatility (or, in other words close boiling points) this vapour–liquid envelope

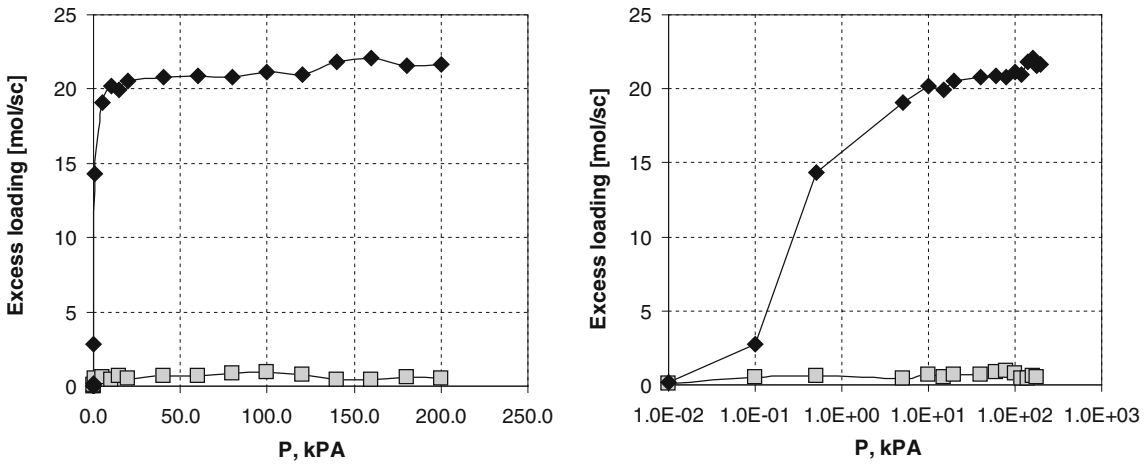

Fig. 6 Adsorption isotherms (number of molecules per simulation cell as a function of pressure) for a binary mixture of *n*-heptane (*grey squares* and *lines*) and i-octane (*black diamonds* and *lines*) in 10 Å slit pore at 390 K. The mixture corresponds to 0.89 mol fraction of i-octane. *Right panel* shows the data using the logarithmic pressure scale

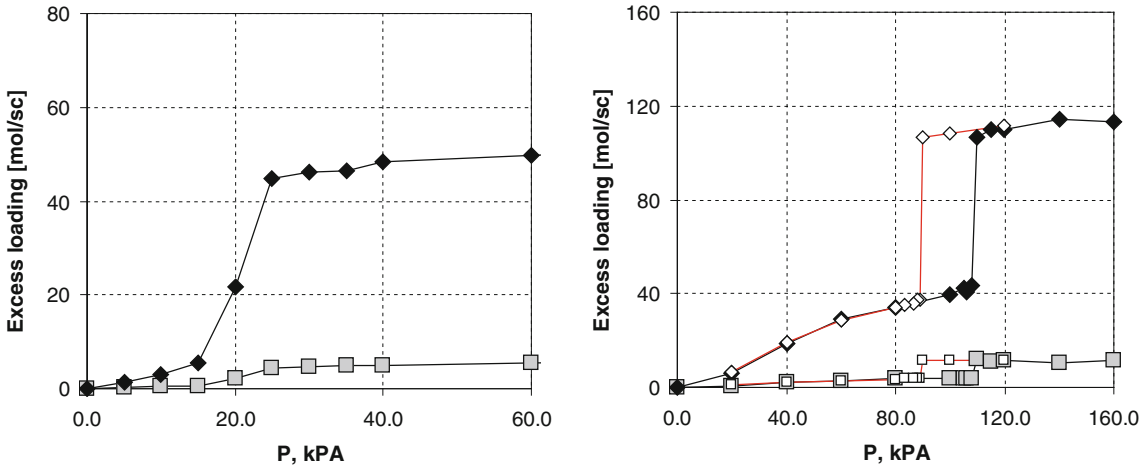

Fig. 7 Adsorption isotherms (number of molecules per simulation cell as a function of pressure) for a binary mixture of *n*-heptane (*grey squares* and *lines*) and i-octane (*black diamonds* and *lines*) in 20 Å slit pore (on the *left*) and 40 Å slit pore (on the *right*) at 390 K. The mixture corresponds to 0.89 mol fraction of i-octane. For 40 Å pore desorption hysteresis is also shown with *white squares* and *red lines* for *n*-heptane and *white diamonds* and *red lines* for i-octane, respectively (Color figure online)

becomes narrow, and the differences in the compositions of the equilibrium vapour and liquid phases are small.

We note here that under conditions of interest the relative *n*-heptane–i-octane volatility barely deviates from one (1.04). The dew and bubble points of the bulk binary mixture with 0.89 mol fraction of i-octane are very close to each other at about 164 kPa, and the composition of the gas phase is essentially the same as the composition of the liquid phase at these points. Given that confinement tends to shrink phase envelopes even further we should not expect any strong manifestations of the two phase envelope for this system.

We now turn to the adsorption isotherms for this binary mixture at 390 K and pressures up 160 kPa, which are shown in Figs. 6 and 7. There are several interesting trends to observe. Similar to the single component case, adsorption in a 10 Å pore corresponds to the capillary filling regime. In larger pores capillary condensation occurs in these systems at pressures close to the single component i-octane capillary condensation. This is particularly evident for the 40 Å, where capillary condensation occurs at a total pressure of 110 kPa (113 kPa for single component i-octane). Figure 8 illustrates the states of the system immediately before and after the condensation, and strong layering at the walls before the condensation is clearly seen. For 40 Å, we also explore desorption hysteresis by reversing the adsorption process at high loading point. The hysteresis loop is observed for both species and the location of the desorption transition (89 kPa) is somewhat lower than that for the single component i-octane

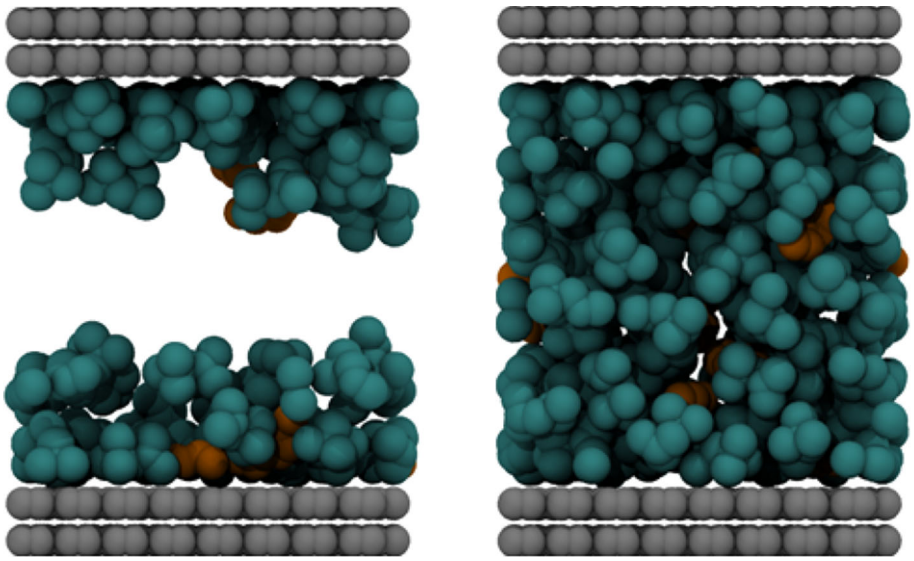

Fig. 8 Computer visualization of the state of 40 Å slit pore immediately before and after condensation of a binary mixture of i-octane (*cyan*) and *n*-heptane (*orange*) at 390 K. Atoms of the walls, shown in *grey*, are slightly scaled down for better visualization. Only two out of six walls on each side are shown (Color figure online)

desorption (98.75 kPa). Again, we emphasize here that both adsorption and desorption transitions observed here for 40 Å pore are hysteresis transitions and neither of the branches corresponds to the true location of the confined vapour–liquid equilibrium.

Finally, we turn our attention to the key issue of this article, which is possible preferential adsorption of branched alkanes versus linear alkanes in carbonaceous slit pores. This behaviour is best characterized by adsorption selectivity:

$$S_{(\mathrm{o/h})} = \frac{x_o/x_n}{y_o/y_n} \tag{2}$$

where $S_{(\mathrm{o/h})}$ is selectivity of i-octane (o) over *n*-heptane (n), and x_i and y_i are the mole fractions of component i in the adsorbed and gas phase, respectively. As has been already discussed, selectivity isotherms even for simpler species such as methane and ethane can exhibit a number of non-trivial effects associated with how molecules arrange themselves in narrow slit pores. For the mixture considered here, this property is plotted in Fig. 9. We also note here, that in order to improve statistics we consider $3 \times 3 \times 1$ replicas of the simulation system in the periodic boundary conditions for the 10 Å pore. In larger pores, modest selectivity towards i-octane can be observed (despite some scattering of data, in 20 Å, it is 1.15 ± 0.13 and in 40 Å pore, it is 1.20 ± 0.10, averaged over the whole pressure range). However, in the smaller 10 Å pore there is a strong preferential adsorption of i-octane with selectivity more than three at lower pressures diminishing to about two at higher pressures. This behaviour is a result of the packing effects in 10 Å pores and lack of compatibility of this pore size with the multilayer normal alkane adsorption. This dramatic increase in selectivity in narrow pores of a certain range, compared to larger pores, is in agreement with the previous observations by Cracknell et al. (1994) and Tan and Gubbins (1992). The selectivity isotherm for 10 Å shows some features (maximum and then diminishing tail) of type I selectivity isotherm according to Tan and Gubbins classification, but given the degree of scattering of the data, this requires further investigation. Furthermore, for the larger pores, selectivity before and after capillary condensation have essentially the same values (within the error of the calculation) and thus there is no additional enhancement of the selectivity in the adsorbed vapour phase as has been noted by Heffelfinger and co-workers for argon/krypton mixtures in cylindrical CO_2 pore (Heffelfinger et al. 1989).

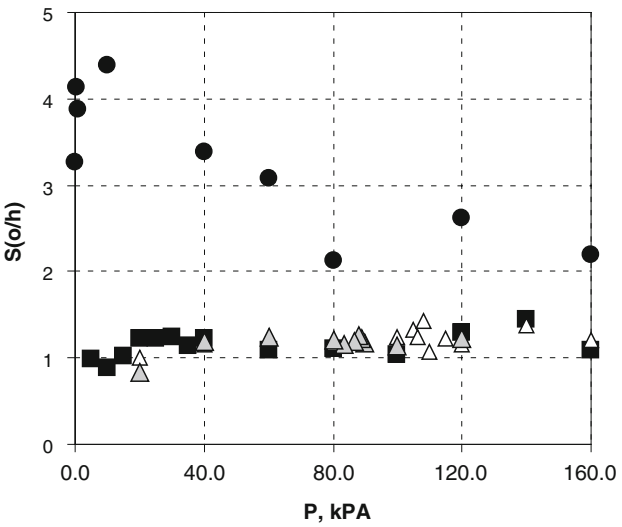

Fig. 9 Selectivity adsorption isotherms for i-octane-*n*-heptane mixture at 390 K (composition of the mixture corresponds to 0.89 mol fraction of i-octane). *Black squares* are for 20 Å pore, *grey* and *open triangles* are for the adsorption and desorption branches in 40 Å pore, respectively, and *black circles* are for 10 Å pore. Selectivity of the mixture is defined in the text

4 Conclusions

Here we presented a computational study of linear and branched alkane adsorption in slit pores of several sizes, representing a simple model of carbonaceous engine deposits. Depending on the pore size, capillary filling and capillary condensation mechanisms of adsorption were observed for *n*-heptane, *n*-octane and i-octane. Adsorption isotherms for larger alkanes in 40 Å also exhibit a pronounced hysteresis loop. Binary mixture adsorption studies revealed a preference for the adsorption of i-octane over *n*-heptane in pores of all sizes considered here. However, in smaller pores, these effects are dramatically enhanced due to the packing effects. This suggests that accurate characterization of the structure of the deposits (their porosity and PSD) is important in assessing their overall impact on the performance of the engine via selective adsorption mechanism. From the first impression, adsorption behaviour of a binary mixture can be represented as a linear combination of single component adsorption isotherms. This invites a further investigation to assess whether these systems, including their selectivity behaviour, can be correctly described using some simplified approach, similar in spirit to the ideal adsorption solution theory (IAST) (Myers and Prausnitz 1965). Further studies are also required to understand the transport mechanisms of these species in the deposits (as these processes can be very slow in micropores) and behaviour of truly multicomponent mixtures, more accurately reflecting real fuels. Finally, we note that the cyclic nature of the processes in the engine is very important for the extent of adsorption uptake and at the same time is very difficult to properly take into account. Fuel components adsorbed at the first cycle may partially desorb at the next cycle or participate in reactions contributing to the growth of the deposits. At the moment this study is only the first step focusing on the equilibrium adsorption. The next step should be a more accurate picture of the dynamics of the process, however it is a highly non-trivial challenge.

Acknowledgments This work has made use of the resources provided by the Edinburgh Compute and Data Facility (ECDF) (http://www.ecdf.ed.ac.uk/). The ECDF is partially supported by the DIKT initiative (http://www.edikt.org.uk). The authors would like to thank Shell Global Solutions for providing the CCD and IVD samples and for funding this project. LS would also like to thank Prof. Berend Smit for an alternative simulation package used to validate simulations results for branched alkanes.

References

Cracknell, R.F., Nicholson, D.: Grand canonical Monte Carlo study of Lennard-Jones mixtures in slit pores. Part 3.-Mixtures of two molecular fluids: ethane and propane. J. Chem. Soc. Faraday Trans. **90**(11), 1487–1493 (1994)

Cracknell, R.F., Nicholson, D., Quirke, N.: A Grand Canonical Monte-Carlo Study of Lennard-Jones Mixtures in Slit Pores; 2: mixtures of two centre ethane with methane. Mol. Simul. **13**(3), 161–175 (1994)

Frenkel, D., Smit, B.: Understanding molecular simulations from algorithms to applications. Academic Press, London (2002)

Davies, G.M., Seaton, N.A.: Development and validation of pore structure models for adsorption in activated carbons. Langmuir **15**(19), 6263–6276 (1999)

Davies, G.M., Seaton, N.A., Vassiliadis, V.S.: Calculation of pore size distributions of activated carbons from adsorption isotherms. Langmuir **15**(23), 8235–8245 (1999)

Do, D.D., Do, H.D.: Pore characterization of carbonaceous materials by DFT and GCMC simulations: a review. Adsorpt. Sci. Technol. **21**(5), 389–423 (2003)

Gelb, L.D., Gubbins, K.E., Radhakrishnan, R., Sliwinska-Bartkowiak, M.: Phase separation in confined systems. Rep. Prog. Phys. **62**(12), 1573–1659 (1999)

Gupta, A., Chempath, S., Sanborn, M.J., Clark, L.A., Snurr, R.Q.: Object-oriented programming paradigms for molecular modeling. Mol. Simul. **29**(1), 29–46 (2003)

Heffelfinger, G.S., Tan, Z., Gubbins, K.E., Marconi, U.M.B., Swol, F.V.: Lennard-Jones Mixtures in a Cylindrical Pore. A comparison of simulation and density functional theory. Mol. Simul. **2**(4–6), 393–411 (1989)

Heywood, J.B.: Internal combustion engine fundamentals. McGraw-Hill, New York (1988)

Houser, K.R., Crosby, T.A.: The Impact of Intake Valve Deposits on Exhaust Emissions. SAE Technical Paper No. 922259 (1992)

Kalghatgi, G.T.: Deposits in gasoline engines: a literature review. SAE (N. 902105) (1990)

Kalghatgi, G.T.: Combustion chamber deposits in spark-ignition engines: a literature review. SAE (952443) (1995)

Kalghatgi, G.T.: Combustion chamber deposits and knock in a sprak ignition engine-some additive and fuel effects. SAE (N. 962009) (1996)

Li, Y., Yu, Y., Zheng, Y., Li, J.: Vapor-liquid equilibrium properties for confined binary mixtures involving CO_2, CH_4, and N_2 from Gibbs ensemble Monte Carlo simulations. Sci. China Chem. **55**(9), 1825–1831 (2012)

Macedonia, M.D., Maginn, E.J.: Pure and binary component sorption equilibria of light hydrocarbons in the zeolite silicalite from grand canonical Monte Carlo simulations. Fluid Phase Equilib. **160**, 19–27 (1999)

Martin, M.G., Siepmann, J.I.: Transferable potentials for phase equilibria. 1. United-atom description of n-alkanes. J. Phys. Chem. B **102**(14), 2569–2577 (1998)

Martin, M.G., Siepmann, J.I.: Novel configurational-bias Monte Carlo method for branched molecules. Transferable potentials for phase equilibria. 2. United-atom description of branched alkanes. J. Phys. Chem. B **103**(21), 4508–4517 (1999)

Myers, A.L., Prausnitz, J.M.: Thermodynamics of mixed-gas adsorption. AIChE J. **11**(1), 121–127 (1965)

Pinto da Costa, J.M.C., Cracknell, R.F., Sarkisov, L., Seaton, N.A.: Structural characterization of carbonaceous combustion-chamber deposits. Carbon **47**(14), 3322–3331 (2009)

Pinto da Costa, J.M.C., Cracknell, R.F., Seaton, N.A., Sarkisov, L.: Towards predictive molecular simulations of normal and branched alkane adsorption in carbonaceous engine deposits. Carbon **49**(2), 445–456 (2011)

Ravikovitch, P.I., Vishnyakov, A., Russo, R., Neimark, A.V.: Unified approach to pore size characterization of microporous carbonaceous materials from N_2, Ar, and CO_2 adsorption isotherms. Langmuir **16**(5), 2311–2320 (2000)

Sarkisov, L., Monson, P.A.: Hysteresis in Monte Carlo and molecular dynamics simulations of adsorption in porous materials. Langmuir **16**(25), 9857–9860 (2000)

Sarkisov, L., Monson, P.A.: Modeling of adsorption and desorption in pores of simple geometry using molecular dynamics. Langmuir **17**(24), 7600–7604 (2001)

Seaton, N.A., Walton, J.P.R.B., Quirke, N.: A new analysis method for the determination of the pore size distribution of porous carbons from nitrogen adsorption measurements. Carbon **27**(6), 853–861 (1989)

Severson, B.L., Snurr, R.Q.: Monte Carlo simulation of n-alkane adsorption isotherms in carbon slit pores. J. Chem. Phys. **126**(13), 134708 (2007)

Shibata, G., Nagaishi, H., Oda, K.: Effect of intake valve deposits and Gasoline composition on SI engine performance. SAE Technical Paper No. 922263 (1992)

Shu, G., Dong, L., Liang, X.: A review of experimental studies on deposits in the combustion chambers of internal combustion engines. Int. J. Engine Res. **13**(4), 357–369 (2012)

Singh, S.K., Sinha, A., Deo, G., Singh, J.K.: Vapor-liquid phase coexistence, critical properties, and surface tension of confined alkanes. J. Phys. Chem. C **113**(17), 7170–7180 (2009)

Snurr, R.Q., Bell, A.T., Theodorou, D.N.: Prediction of adsorption of aromatic hydrocarbons in silicalite from grand canonical Monte Carlo simulations with biased insertions. J. Phys. Chem **97**(51), 13742–13752 (1993)

Talu, O., Myers, A.L.: Molecular simulation of adsorption: gibbs dividing surface and comparison with experiment. AIChE J. **47**(5), 1160–1168 (2001)

Tan, Z., Gubbins, K.E.: Selective adsorption of mixtures in slit pores - a model of methane ethane mixtures in carbon. J. Phys. Chem. **96**(2), 845–854 (1992)

Vega, L.F.: Theoretical and computational chemistry. In: Balbuena, P.B., Seminario, J.M. (eds.) Nanomaterials: design and simulation, pp. 101–126. Elsevier, Amsterdam (2007)

Zerda, T.W., Yuan, X., Moore, S.M., Leon, C.: Surface area, pore size distribution and microstructure of combustion engine deposits. Carbon **37**(12), 1999–2009 (1999)